Docking Controller for Autonomous Aerial Refueling With Adaptive Dynamic Surface Control

JIAZHENG WU[ID], HUANGDI LUO, AND JIANLIANG AI
Department of Aeronautics and Astronautics, Fudan University, Shanghai 200433, China
Corresponding author: Jiazheng Wu (jzwu14@fudan.edu.cn)

ABSTRACT The docking controller for autonomous aerial refueling (AAR) is intractable considering the high precision requirement and the complex disturbances of multiple environment flows. To solve the problems in the docking phase of AAR, such as the uncertainties of the aerodynamic parameters of receiver aircraft and the disturbances acting on the receiver aircraft, an adaptive dynamic surface control (ADSC) scheme based on radical basis function neural network (RBF-NN) is presented in this paper. Firstly, a nonlinear model of longitudinal dynamics of the receiver aircraft relative to the tanker aircraft is established, which incorporates the tanker vortex term. Secondly, a nonlinear strict-feedback form is introduced to design an adaptive dynamic surface controller with RBF-NN. Thirdly, the upper bounds of the ''total disturbances'' are estimated with the adaptive law, and the uncertain aerodynamic parameters of receiver aircraft are estimated with RBF-NN. It is proved that the proposed controller can guarantee the uniform boundedness of all the signals in the closed-loop system using Lyapunov theory. Finally, simulation results demonstrate the effectiveness of the proposed controller for the docking control of AAR.

INDEX TERMS Autonomous aerial refueling, docking controller, adaptive dynamic surface control, RBF neural network.

I. INTRODUCTION

An interest over the last decade in developing unmanned aerial systems' (UAS) technologies has prompted research into methods for AAR processes [1]. The AAR techniques make new missions and capabilities possible for future unmanned aerial vehicles (UAVs) through extending the range and endurance [2], [3]. Two types of aerial refueling methods, probe-drogue refueling (PDR) and boom-receptacle refueling (BRR), are mainly employed currently, among which PDR method is considered to be more flexible and compact than BRR method [1], [4]. The PDR method can be applied to different aircrafts, different refueling speeds, and multiple aircraft refueling tasks, therefore it is suitable for UAV aerial refueling operation. The PDR method includes five phases. Docking phase is the most critical and difficult one, which directly affects the success of the whole AAR operation [5], [6]. PDR docking controller design aims at achieving automatic maneuvers of the receiver aircraft (manned or unmanned) to send the probe to the close

The associate editor coordinating the review of this manuscript and approving it for publication was Ming Xu[ID].

proximity of the moving drogue and maintain the probe there. Two main reasons make PDR docking a difficult task. The first reason is that the system model in the docking phase is a multi-input multi-output (MIMO) high order system with strong nonlinearity, which is complex for control design. Moreover, the drogue is susceptible to the disturbances, thus it is hard for the probe on the receiver aircraft to capture the moving drogue [6], [7]. B. Mario *et al.* developed the robotic pseudo-dynamic testing (RPsDT) method with hardware-in-loop experiment for the PDR docking, and got insight of the nonlinear characteristics of the drogue and the contact behavior [8]. The second reason is that the precision requirement of the PDR docking control is high. The tracking error and the relative velocity between two aircrafts should be within a small range [9]. Therefore, the PDR docking controller design has always been significant and challenging.

In recent years, with the development of UAVs and AAR, many researches have been carried out on the control of receiver aircraft during AAR operation. The most commonly used method is linear quadratic regulator (LQR) [10]–[13], which is linearized model based and the optimal feedback gain matrix can be obtained. In [11], a position tracking

controller is designed using gain scheduling technique and optimal LQR control, where the anti-disturbance ability for the unknown disturbances is not considered in the controller design. In [12], machine vision based algorithms are implemented to detect the relative position and orientation between the UAV and the tanker. Another linear model based method known as L1 adaptive control methodology is applied to receiver tracking control in AAR [14], [15], and neural network (NN) is also utilized to estimate the system uncertainties.

Some improved work is then carried out based on the nonlinear system model. Also, the complex disturbances are taken into consideration. In [16], [17], the authors use the nonlinear dynamic inversion (NDI) with some uncertainty compensation technique to design the receiver tracking controller. The NDI-based controllers are only designed in the attitude loop, and cannot guarantee the performance in path and position loop. Recently, active disturbance rejection control (ADRC) [18]–[20] has received much attention in AAR control research. Z. Su *et al.* use back-stepping technique to divide the dynamic model of the receiver into five loops and employ ADRC for the docking controller design [18]. They take the system nonlinearities, uncertainties, and disturbances as the "total disturbances" which are estimated and compensated by extended state observer (ESO). In the position loop, the proper reference path angle is determined by fuzzy logic. In [21], Z. Su *et al.* utilize high order sliding mode observer (HOSMO) to achieve better estimation effects. Moreover, some modern control methods are also studied for their application in AAR control, such as: fault-tolerant control [22], [23] and terminal iterative learning control (TILC) [6], [24].

Although there are many approaches available for the docking control of AAR, this problem is still open. For nonlinear systems with uncertainty and external disturbances, adaptive dynamic surface control (ADSC) is one of the important methods to design controllers during these years. ADSC is based on back-stepping technique, but simplifies it by introducing the first-order filters and avoids the calculation of derivatives of the virtual control signals [25]. Considering NNs have an inherent ability of learning nonlinear dynamics and handling both unknown uncertainties as well as time-varying disturbances, it is also incorporated into ADSC design scheme [26]. ADSC is developed and achieve satisfactory results in multiple control research areas, such as nonlinear hypersonic air vehicle path following [27]–[29], formation of autonomous ships [30], [31], mobile wheeled inverted pendulum, and mobile robots control [32], [33].

Inspired by aforementioned work of ADSC research, in this paper, a radical basis function neural network (RBF-NN) based ADSC approach is applied to the controller of the receiver aircraft, which has uncertain nonlinear dynamics and subjects to the disturbances. RBF-NN is utilized to accommodate the uncertain dynamics. The stability of the close-loop system is proven via Lyapunov theory. The main contributions of this paper are listed as follows:
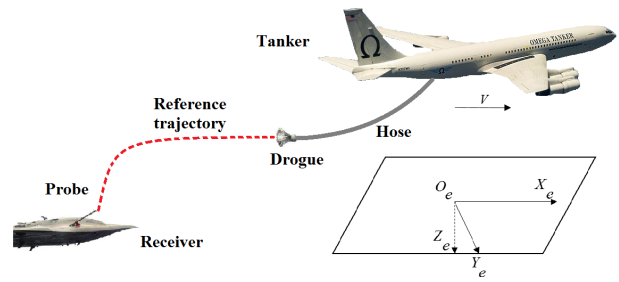

FIGURE 1. The configuration of PDR system.

1) The multiple environment flows' influence on the receiver and the drogue's motion are both considered during the docking controller design, and a novel ADSC flight controller with RBF-NN technique is proposed for AAR.
2) The receiver model is divided into two subsystems and written in strict-feedback nonlinear forms, an adaptive algorithm combining RBF-NN and dynamic surface control (DSC) is designed, which can handle both the internal uncertainties and external disturbances, namely, it doesn't depend on the accurate model of the receiver aircraft which is not available in practice.

The rest of this paper is organized as follows. Section II describes the system model and the control object. Section III presents the design of the NN-ADSC controller and proves its stability. The numerical simulation is performed in Section IV to illustrate the effectiveness of the proposed method. Section V outlines the concluding remarks and future works.

II. MATHEMATICAL MODEL AND PROBLEM STATEMENT

A typical PDR system is presented in Fig. 1, which consists of a flexible hose, a cone-shaped drogue, and a rigid probe. The hose trails behind and below the tanker, the drogue is mounted at the end of the hose, and the probe is equipped on the receiver protruding from its nose [6]. During the refueling operation, the tanker aircraft is always flying in level flight, namely, the tanker makes a uniform linear motion with constant speed V_T and altitude H_T. The docking control task is to control the receiver aircraft to maneuver from the pre-contact position to the contact position along the reference trajectory to establish a link-up between the probe and the drogue for fuel transfer. Thus, the controller design is focused on the receiver aircraft.

A. DYNAMICS OF THE RECEIVER AIRCRAFT

As the receiver aircraft makes only forward and vertical maneuver during the docking phase from the pre-contact position to the contact position in $X_e Z_e$-plane, the longitudinal dynamics model of the receiver aircraft with respect to the tanker aircraft is derived and adopted from [11]. The model is comprised of six longitudinal state variables $\begin{bmatrix} x & V & z & \gamma & \theta & q \end{bmatrix}^T$ and two control input variables $\begin{bmatrix} \delta_e & \delta_T \end{bmatrix}^T$, where V is the

velocity of the receiver aircraft, x and z are the coordinates of the receiver aircraft expressed in the tanker body frame, γ is the flight path angle, θ is the pitch angle, α is the angle of attack, and q is the pitch rate. It should be noted that $\theta = \gamma + \alpha$ when only the longitudinal dynamics is considered. The model is described as:

$$\dot{x} = V\cos\gamma - V_T + w_x\cos\theta + w_z\sin\theta \tag{1}$$

$$\dot{V} = -\frac{\mathcal{D}}{m} + \frac{\mathcal{T}\cos\alpha}{m} - (\dot{w}_x + qw_z)\cos\alpha$$
$$+ (qw_x - \dot{w}_z)\sin\alpha - g\sin\gamma \tag{2}$$

$$\dot{z} = -V\sin\gamma + w_z\cos\theta - w_x\sin\theta \tag{3}$$

$$\dot{\gamma} = -\frac{-\mathcal{L} + mg\cos\gamma - \mathcal{T}\sin\alpha}{mV}$$
$$+ \frac{m(qw_x - \dot{w}_z)\cos\alpha + m\dot{w}_x\sin\alpha}{mV}$$
$$+ \frac{mgw_z\sin\alpha}{mV} \tag{4}$$

$$\dot{\theta} = q \tag{5}$$

$$\dot{q} = \frac{\mathcal{M}}{I_y} \tag{6}$$

where g, m, and I_y represent the gravity, mass, and inertial constant of the receiver aircraft, respectively. V_T is the velocity of the tanker. $\mathcal{L}$ and $\mathcal{D}$ are the lift and drag force. $\mathcal{M}$ is the pitch moment along the axis of the body frame. $\mathcal{T}$ is the thrust. The explicit forms of these variables will be given in Appendix A.

AAR is one type of tight formation flight, where the receiver aircraft is in close proximity behind the tanker aircraft. The wake vortex generated by the tanker can sharply influence the dynamics of the receiver. Hence, the wake vortex should be considered in the model of the receiver for control. In this paper, the scheme in [34] is adopted to generate the vortex term in (1) – (4). w_x, w_z are the induced wind velocities along the axis of the receiver body frame, and the $\dot{w}_x, \dot{w}_z$ represent the wind gradients. The technique takes the relative separation and orientation between the two aircraft, geometrical characteristics as well as the velocity into consideration. A weighted averaging scheme is implemented to compute the effective wind and wind gradients as uniform approximations which are nonuniform. Once a fairly reasonable approximation is achieved, the vortex term can be explicitly added in the receiver dynamics which is more direct and computationally efficient than other methods. The details about the scheme for estimating the vortex-effect on the receiver could be found in [34].

B. DYNAMICS TRANSFORMATION
From the longitudinal model of the receiver (1) – (6), it can be inferred that the main contribution in the change of the forward distance with respect to the tanker is from the throttle control variable δ_T and the vertical change is related mainly to the elevator deflection δ_e. Separate control design for two channels may, therefore, be carried out. In order to employ ADSC in the docking controller design, the model of the

receiver should be written in strict-feedback form. Dynamics transformation is implemented for two subsystems, forward subsystem and altitude subsystem.

1) FORWARD SUBSYSTEM

$$\dot{x} = f_1 + g_1 V \tag{7}$$

$$\dot{V} = f_2 + g_2\delta_T \tag{8}$$

where the explicit forms for f_1, g_1, f_2, g_2 are given in Appendix B.

2) ALTITUDE SUBSYSTEM
In order to obtain altitude subsystem in strict-feedback form, we make undermentioned assumptions.

Assumption 1: The thrust term $T\sin\alpha$ in (4) can be neglected since it is greatly smaller than the lift force L.

Then the strict-feedback form equations of altitude subsystem are written as:

$$\dot{z} = f_3 + g_3\gamma \tag{9}$$

$$\dot{\gamma} = f_4 + g_4\theta \tag{10}$$

$$\dot{\theta} = q \tag{11}$$

$$\dot{q} = f_6 + g_6\delta_e \tag{12}$$

where the explicit forms for f_3, g_3, f_4, g_4, f_6, g_6 are also presented in Appendix B.

Assumption 2: f_i and g_i are uncertain smooth functions. From the explicit forms of g_i in Appendix B, it is obvious that they are all bounded, namely, there exist constants g_{im}, g_{iM} and g_{ic} such that $0 < g_{im} \leq |g_i| \leq g_{iM}$, $|\dot{g}_i| \leq g_{ic}$, $i = 1, \cdots, 6$.

Assumption 3: The reference signal x_d and z_d is smooth and available, and $x_d \in \Omega_x = \{x_d | x_d^2 + \dot{x}_d^2 + \ddot{x}_d^2 \leq B_x\}$, $z_d \in \Omega_z = \{z_d | z_d^2 + \dot{z}_d^2 + \ddot{z}_d^2 \leq B_z\}$.

C. PROBLEM STATEMENT
1) DROGUE MOTION
Under the effect of nonuniform tanker vortex, the hose-drogue system will eventually stabilize at an equilibrium position. Also, the drogue position fluctuates around its equilibrium position due to the atmospheric turbulence whose characteristics are shown in Fig. 2. The drogue motion model in [35] is employed here, whose corresponding state space representation is:

$$\Delta\dot{x}_d(t) = \mathbf{A}_d\Delta x_d(t) + \mathbf{B}_dw_g(t) \tag{13}$$

$$\Delta y_d(t) = \mathbf{C}_d\Delta x_d(t) \tag{14}$$

where $\Delta x_d(t) = [\Delta x_d(t), \Delta y_d(t), \Delta z_d(t), \Delta\dot{x}_d(t), \Delta\dot{y}_d(t), \Delta\dot{z}_d(t)]^T$, $\Delta y_d(t) = [\Delta x_d(t), \Delta y_d(t), \Delta z_d(t)]^T$, and $\Delta x_d(t)$, $\Delta y_d(t)$, $\Delta z_d(t)$ represent the drogue position error from its equilibrium point along each axis, respectively.

2) CONTROL OBJECTIVE
PDR docking controller design aims at achieving automatic maneuvers of the receiver from pre-contact position to the
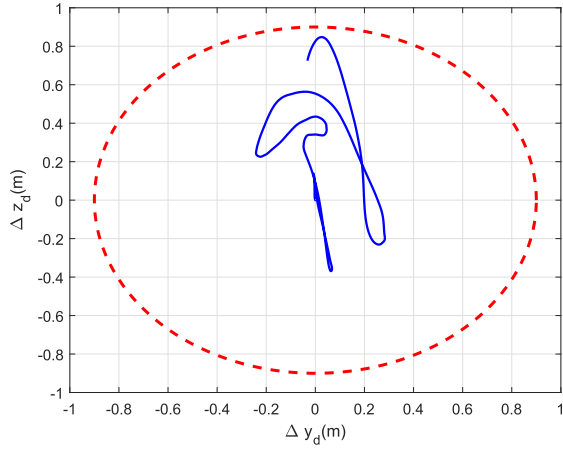
FIGURE 2. Drogue motion around its equilibrium position.

contact position, sending the probe to the close proximity of the moving drogue and maintain the probe there. In each docking operation, after correcting the vertical position error, the receiver drives the probe to approach the drogue with a slow constant speed in x_e direction until the probe hits the central plane of the drogue. The docking process lasts from 0 to t_f which is expected to be equal to t_{dock} (desired docking moment). At this moment, a radial error between the drogue and the probe is defined as:

$$e_{dock} \triangleq \|[y_d(t_f) \quad z_d(t_f)]^T - [y(t_f) \quad z(t_f)]^T\| \quad (15)$$

where $y_d(t)$, $z_d(t)$, $y(t)$, $z(t)$ are the position of drogue and probe with respect to the cruise state of the receiver, respectively. Since the docking error is inevitable due to the disturbances, a threshold radius R_c is utilized to evaluate docking performance. Thus, the control objective is $x(t_f) \rightarrow x_d(t_f)$ and $e_{dock} < R_c$.

3) REFERENCE TRAJECTORY DESIGN

In order to achieve a successful docking, a safe and smooth trajectory from the starting position (pre-contact) to the final position (contact) needs to be generated. Controlling the receiver to track the reference trajectory can avoid actuator saturation and large overshoot in the docking process.

There are two important requirements of the reference trajectory generated for the PDR docking. The first and foremost requirement is to ensure the safety of the aircraft and the refueling unit. Namely, there should not be any risk of collision between two aircrafts and the hose-drogue system. Furthermore, the motion of the drogue under disturbances should not necessarily disturb the whole trajectory design. Thus, the vertical position error between the probe and drogue is corrected in the first part of the trajectory and the drogue's motion should be considered in final part of the trajectory. Secondly, the generated trajectory should be feasible, namely realizable within the dynamics constraints of the receiver. To satisfy the second requirement, a continuously differentiable smooth trajectory is introduced.
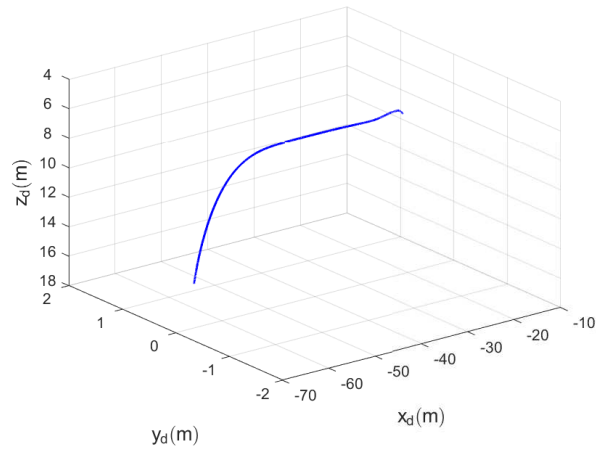

FIGURE 3. Reference trajectory of the receiver.

For x direction, a high order polynomial trajectory is established as:

$$x_{ref}(t) = a_{11}t^4 + a_{12}t^5 + a_{13}t^6 + a_{14}t^7 \quad (16)$$

where a_{11}, a_{12}, a_{13}, and a_{14} are determined by following boundary conditions:

$$x_{ref}(t_f) = x_d(0), \quad \frac{dx_{ref}}{dt}(t_f) = 0,$$
$$\frac{d^2x_{ref}}{dt^2}(t_f) = 0, \quad \frac{d^3x_{ref}}{dt^3}(t_f) = 0 \quad (17)$$

For z direction, trajectory is divided into two parts, similar polynomial trajectory with x direction is used in first part (from 0 to t_1) which aims to correct the z direction position error relative to drogue's equilibrium position:

$$z_{ref}(t) = a_{21}t^4 + a_{22}t^5 + a_{23}t^6 + a_{24}t^7, \quad 0 \le t \le t_1 \quad (18)$$

where a_{21}, a_{22}, a_{23}, and a_{24} are determined by following boundary conditions:

$$z_{ref}(t_1) = z_d(0), \quad \frac{dz_{ref}}{dt}(t_1) = 0,$$
$$\frac{d^2z_{ref}}{dt^2}(t_1) = 0, \quad \frac{d^3z_{ref}}{dt^3}(t_1) = 0 \quad (19)$$

In second part, the motion of the drogue is incorporated into the reference trajectory:

$$z_{ref}(t) = z_d(0) + K_{ref}(t)\Delta z_d(t), \quad t_1 \le t \quad (20)$$

where K_{ref} is the weight coefficient increasing from 0 to 1 over time. In this paper, we suppose that before declaring docking, the drogue fluctuates around its equilibrium position and both the receiver and the tanker have synchronized velocity in the same direction. Then a designed reference trajectory for the receiver from pre-contact position to the contact position is shown in Fig. 3.
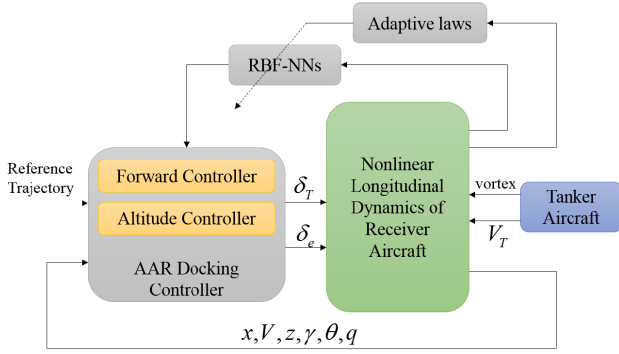
FIGURE 4. The architecture of the control scheme for receiver.

FIGURE 5. The structure of RBF-NN.

III. CONTROL STRATEGY

In this section, we develop a NN-ADSC controller for reference trajectory tracking of the receiver, to accomplish the goal of AAR docking. The recursive design procedure breaks into several steps for two subsystems. During the controller design, RBF-NNs are employed for a nonlinear function approximation of $f_i, g_i, i = 1, \cdots, 6$. The overall control structure is illustrated in Fig. 4. The stability analysis of the controlled closed-loop system will be carried out via Lyapunov theory.

A. RBF NEURAL NETWORKS

In this paper, the RBF-NNs are employed to approximate the unknown nonlinearity f with the following form [26], [28]:

$$\hat{f}(\boldsymbol{x}) = \hat{\boldsymbol{W}}^{\mathrm{T}}\boldsymbol{\xi}(\boldsymbol{x}) \qquad (21)$$

where $\boldsymbol{x} \in R^M$ is the input vector of the RBF-NN, $\hat{f} \in R$ is the RBF-NN output, $\hat{\boldsymbol{W}} \in R^N$ is the weight vector, $\boldsymbol{\xi}(\boldsymbol{x}) \in R^N$ is a vector valued function of the inputs, and N is the number of the RBF-NN nodes. The components of $\boldsymbol{\xi}(\boldsymbol{x})$ are basis functions denoted by $\rho_i(\boldsymbol{x}), i = 1, \cdots, N$. A commonly used basis function is the so-called Gaussian function of the following form:

$$\rho_j(\boldsymbol{x}) = \frac{1}{\sqrt{2\pi}\sigma_j}\exp(-\frac{\|\boldsymbol{x} - \boldsymbol{c}_j\|^2}{2\sigma_j^2}), \quad j = 1, \cdots, N \quad (22)$$

where $\boldsymbol{c}_j$ is an M-dimensional vector representing the center of the jth basis function and σ_j is a real number called the width of the basis function. The structure of the RBF-NN is shown in Fig. 5.

According to the approximation property of the RBF-NNs [36], [37], given any continuous real valued function on a compact set $f : \Omega \to R, \Omega \in R^M$, and an arbitrary $\varepsilon_m > 0$, for some sufficiently large number of RBF-NN nodes N, there exists an ideal weight vector $\boldsymbol{W}^* \in R^N$ such that the RBF-NN $\boldsymbol{W}^{*\mathrm{T}}\boldsymbol{\xi}(\boldsymbol{x})$ can approximate the given function f with the approximation error bounded by ε_m, i.e.

$$f(\boldsymbol{x}) = \boldsymbol{W}^{*\mathrm{T}}\boldsymbol{\xi}(\boldsymbol{x}) + \varepsilon^* \qquad (23)$$

with $|\varepsilon^*| \le \varepsilon_m$. Since $\boldsymbol{W}^*$ is unknown, we need to estimate $\boldsymbol{W}^*$ online, where its estimation is denoted by $\hat{\boldsymbol{W}}$ and an adaptive law is developed to update $\hat{\boldsymbol{W}}$.
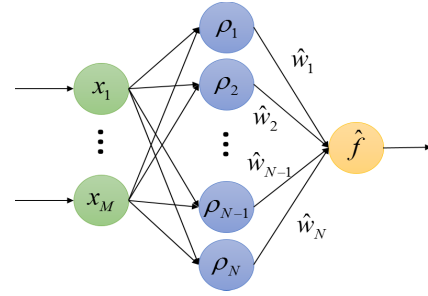
B. FORWARD SUBSYSTEM CONTROL DESIGN

Step 1. Define $S_1 \triangleq x - x_d$. The dynamics of the forward distance error is written as:

$$\begin{aligned} \dot{S}_1 &= \dot{x} - \dot{x}_d \\ &= f_1 + g_1 V - \dot{x}_d \\ &= g_1(g_1^{-1}f_1 + V - g_1^{-1}\dot{x}_d) \end{aligned} \qquad (24)$$

Using RBF-NN to approximate the unknown function $g_1^{-1}f_1, g_1^{-1}$ on the compact set Ω_{x1}, we have

$$g_1^{-1}f_1 = \boldsymbol{W}_1^{*\mathrm{T}}\boldsymbol{\xi}_1 + \varepsilon_1^* \qquad (25)$$

$$g_1^{-1} = \boldsymbol{V}_1^{*\mathrm{T}}\boldsymbol{\zeta}_1 + \delta_1^* \qquad (26)$$

where $\boldsymbol{W}_1^*, \boldsymbol{V}_1^*$ are optimal weight vectors, $\boldsymbol{\xi}_1, \boldsymbol{\zeta}_1$ are the basis function vectors, $\varepsilon_1^*, \delta_1^*$ are NN approximation error, and $|\varepsilon_1^*| < \varepsilon_{1m}, |\delta_1^*| < \delta_{1m}$.

A virtual control variable $\bar{V}_d$ is designed as:

$$\bar{V}_d = -k_1 S_1 - \hat{\boldsymbol{W}}_1^{\mathrm{T}}\boldsymbol{\xi}_1 + \hat{\boldsymbol{V}}_1^{\mathrm{T}}\boldsymbol{\zeta}_1\dot{x}_d \qquad (27)$$

where $k_1 > 0$ is the gain parameter, $\hat{\boldsymbol{W}}_1$ is the estimation of $\boldsymbol{W}_1^*$, and $\hat{\boldsymbol{V}}_1$ is the estimation of $\boldsymbol{V}_1^*$.

Introduce a new state variable V_d and let $\bar{V}_d$ pass through a first-order filter with positive time constant τ_2 to obtain V_d

$$\tau_2 \dot{V}_d + V_d = \bar{V}_d, \quad V_d(0) = \bar{V}_d(0). \qquad (28)$$

Define $y_2 \triangleq V_d - \bar{V}_d, S_2 \triangleq V - V_d$. Then, (24) is calculated as:

$$\begin{aligned} \dot{S}_1 &= g_1(g_1^{-1}f_1 + V - g_1^{-1}\dot{x}_d) \\ &= g_1[\boldsymbol{W}_1^{*\mathrm{T}}\boldsymbol{\xi}_1 + \varepsilon_1^* + (-k_1 S_1 - \hat{\boldsymbol{W}}_1^{\mathrm{T}}\boldsymbol{\xi}_1 + \hat{\boldsymbol{V}}_1^{\mathrm{T}}\boldsymbol{\zeta}_1\dot{x}_d) \\ &\quad + y_2 + S_2 - (\boldsymbol{V}_1^{*\mathrm{T}}\boldsymbol{\zeta}_1 + \delta_1^*)\dot{x}_d] \\ &= g_1[-k_1 S_1 - \tilde{\boldsymbol{W}}_1^{\mathrm{T}}\boldsymbol{\xi}_1 + \tilde{\boldsymbol{V}}_1^{\mathrm{T}}\boldsymbol{\zeta}_1\dot{x}_d + y_2 + S_2 \\ &\quad + \varepsilon_1^* - \delta_1^*\dot{x}_d] \end{aligned} \qquad (29)$$

where $\tilde{\boldsymbol{W}}_1 = \hat{\boldsymbol{W}}_1 - \boldsymbol{W}_1^*$ and $\tilde{\boldsymbol{V}}_1 = \hat{\boldsymbol{V}}_1 - \boldsymbol{V}_1^*$.

The adaptive laws of the estimated weight vectors are designed as:

$$\dot{\hat{\boldsymbol{W}}}_1 = \Gamma_1 S_1 \boldsymbol{\xi}_1 - \Gamma_1 \eta_1 \hat{\boldsymbol{W}}_1 \qquad (30)$$

$$\dot{\hat{\boldsymbol{V}}}_1 = \Gamma_{g_1} S_1 \boldsymbol{\zeta}_1 \dot{x}_d - \Gamma_{g_1} \eta_2 \hat{\boldsymbol{V}}_1 \qquad (31)$$

Step 2. The dynamics of the velocity tracking error S_2 is written as:

$$\dot{S}_2 = \dot{V} - \dot{V}_d$$

$$
\begin{aligned}
&= f_2 + g_2\delta_T - \dot{V}_d \\
&= g_2(g_2^{-1}f_2 + \delta_T - g_2^{-1}\dot{V}_d) \qquad (32)
\end{aligned}
$$

Using RBF-NN to approximate the unknown function $g_2^{-1}f_2$, g_2^{-1} on the compact set Ω_{x_2}, we have

$$
g_2^{-1}f_2 = \boldsymbol{W}_2^{*\mathrm{T}}\boldsymbol{\xi}_2 + \varepsilon_2^* \qquad (33)
$$
$$
g_2^{-1} = \boldsymbol{V}_2^{*\mathrm{T}}\boldsymbol{\zeta}_2 + \delta_2^* \qquad (34)
$$

where $\boldsymbol{W}_2^*$, $\boldsymbol{V}_2^*$ are optimal weight vectors, $\boldsymbol{\xi}_2$, $\boldsymbol{\zeta}_2$ are the basis function vectors, ε_2^*, δ_2^* are NN approximation error, and $|\varepsilon_2^*| < \varepsilon_{2m}$, $|\delta_2^*| < \delta_{2m}$.

The control variable δ_T is designed as:

$$
\delta_T = -k_2 S_2 - \hat{\boldsymbol{W}}_2^{\mathrm{T}}\boldsymbol{\xi}_2 + \hat{\boldsymbol{V}}_2^{\mathrm{T}}\boldsymbol{\zeta}_2 \dot{V}_d \qquad (35)
$$

where $k_2 > 0$ is the gain parameter, $\hat{\boldsymbol{W}}_2$ is the estimation of $\boldsymbol{W}_2^*$, and $\hat{\boldsymbol{V}}_2$ is the estimation of $\boldsymbol{V}_2^*$.

Then, (32) is calculated as:

$$
\begin{aligned}
\dot{S}_2 &= g_2(g_2^{-1}f_2 + \delta_T - g_2^{-1}\dot{V}_d) \\
&= g_2[\boldsymbol{W}_2^{*\mathrm{T}}\boldsymbol{\xi}_2 + \varepsilon_2^* + (-k_2 S_2 - \hat{\boldsymbol{W}}_2^{\mathrm{T}}\boldsymbol{\xi}_2 + \hat{\boldsymbol{V}}_2^{\mathrm{T}}\boldsymbol{\zeta}_2\dot{V}_d) \\
&\quad - (\boldsymbol{V}_2^{*\mathrm{T}}\boldsymbol{\zeta}_2 + \delta_2^*)\dot{V}_d] \\
&= g_2[-k_2 S_2 - \tilde{\boldsymbol{W}}_2^{\mathrm{T}}\boldsymbol{\xi}_2 + \tilde{\boldsymbol{V}}_2^{\mathrm{T}}\boldsymbol{\zeta}_2\dot{V}_d + \varepsilon_2^* - \delta_2^*\dot{V}_d] \quad (36)
\end{aligned}
$$

where $\tilde{\boldsymbol{W}}_2 = \hat{\boldsymbol{W}}_2 - \boldsymbol{W}_2^*$ and $\tilde{\boldsymbol{V}}_2 = \hat{\boldsymbol{V}}_2 - \boldsymbol{V}_2^*$.

The adaptive laws of the estimated weight vectors are designed as:

$$
\dot{\hat{\boldsymbol{W}}}_2 = \Gamma_2 S_2\boldsymbol{\xi}_2 - \Gamma_2\eta_3\hat{\boldsymbol{W}}_2 \qquad (37)
$$
$$
\dot{\hat{\boldsymbol{V}}}_2 = \Gamma_{g_2} S_2\boldsymbol{\zeta}_2\dot{V}_d - \Gamma_{g_2}\eta_4\hat{\boldsymbol{V}}_2 \qquad (38)
$$

C. ALTITUDE SUBSYSTEM CONTROL DESIGN

For the altitude subsystem (3)–(6), define the altitude tracking error as $S_3 \triangleq z - z_d$, and the flight path angle command is designed as:

$$
\gamma_d = \frac{-k_{31}S_3 - k_{32}\int S_3 dt + \dot{z}_d}{-V} \qquad (39)
$$

where k_{31}, k_{32} are positive feedback gain and the altitude tracking error is regulated to zero exponentially.

Assumption 4: In AAR docking process, the velocity of the receiver changes in small range and is considered as slow dynamics. For the controller design of altitude subsystem, velocity is approximated as constant, and its derivative is zero.

With assumption 4, $\dot{\gamma}_d$ is calculated as:

$$
\dot{\gamma}_d = \frac{-k_{31}\dot{S}_3 - k_{32}S_3 + \ddot{z}_d}{-V} \qquad (40)
$$

Step 1. Define $S_4 \triangleq \gamma - \gamma_d$. The dynamics of the flight path angle tracking error is written as:

$$
\begin{aligned}
\dot{S}_4 &= \dot{\gamma} - \dot{\gamma}_d \\
&= f_4 + g_4\theta - \dot{\gamma}_d \\
&= g_4(g_4^{-1}f_4 + \theta - g_4^{-1}\dot{\gamma}_d) \qquad (41)
\end{aligned}
$$

Using RBF-NN to approximate the unknown function $g_4^{-1}f_4$, g_4^{-1} on the compact set Ω_{x_4}, we have

$$
g_4^{-1}f_4 = \boldsymbol{W}_4^{*\mathrm{T}}\boldsymbol{\xi}_4 + \varepsilon_4^* \qquad (42)
$$
$$
g_4^{-1} = \boldsymbol{V}_4^{*\mathrm{T}}\boldsymbol{\zeta}_4 + \delta_4^* \qquad (43)
$$

where $\boldsymbol{W}_4^*$, $\boldsymbol{V}_4^*$ are optimal weight vectors, $\boldsymbol{\xi}_4$, $\boldsymbol{\zeta}_4$ are the basis function vectors, ε_4^*, δ_4^* are NN approximation error, and $|\varepsilon_4^*| < \varepsilon_{4m}$, $|\delta_4^*| < \delta_{4m}$.

A virtual control variable $\bar{\theta}_d$ is designed as:

$$
\bar{\theta}_d = -k_4 S_4 - \hat{\boldsymbol{W}}_4^{\mathrm{T}}\boldsymbol{\xi}_4 + \hat{\boldsymbol{V}}_4^{\mathrm{T}}\boldsymbol{\zeta}_4\dot{\gamma}_d \qquad (44)
$$

where $k_4 > 0$ is the gain parameter, $\hat{\boldsymbol{W}}_4$ is the estimation of $\boldsymbol{W}_4^*$, and $\hat{\boldsymbol{V}}_4$ is the estimation of $\boldsymbol{V}_4^*$.

Introduce a new state variable θ_d and let $\bar{\theta}_d$ pass through a first-order filter with positive time constant τ_5 to obtain θ_d

$$
\tau_5\dot{\theta}_d + \theta_d = \bar{\theta}_d, \theta_d(0) = \bar{\theta}_d(0). \qquad (45)
$$

Define $y_5 \triangleq \theta_d - \bar{\theta}_d$, $S_5 triangleq \theta - \theta_d$. Then, (41) is calculated as:

$$
\begin{aligned}
\dot{S}_4 &= g_4(g_4^{-1}f_4 + \theta - g_4^{-1}\dot{\gamma}_d) \\
&= g_4[\boldsymbol{W}_4^{*\mathrm{T}}\boldsymbol{\xi}_4 + \varepsilon_4^* + (-k_4 S_4 - \hat{\boldsymbol{W}}_4^{\mathrm{T}}\boldsymbol{\xi}_4 + \hat{\boldsymbol{V}}_4^{\mathrm{T}}\boldsymbol{\zeta}_4\dot{\gamma}_d) \\
&\quad + y_5 + S_5 - (\boldsymbol{V}_4^{*\mathrm{T}}\boldsymbol{\zeta}_4 + \delta_4^*)\dot{\gamma}_d] \\
&= g_4[-k_4 S_4 - \tilde{\boldsymbol{W}}_4^{\mathrm{T}}\boldsymbol{\xi}_4 + \tilde{\boldsymbol{V}}_4^{\mathrm{T}}\boldsymbol{\zeta}_4\dot{\gamma}_d + y_5 + S_5 \\
&\quad + \varepsilon_4^* - \delta_4^*\dot{\gamma}_d] \qquad (46)
\end{aligned}
$$

where $\tilde{\boldsymbol{W}}_4 = \hat{\boldsymbol{W}}_4 - \boldsymbol{W}_4^*$ and $\tilde{\boldsymbol{V}}_4 = \hat{\boldsymbol{V}}_4 - \boldsymbol{V}_4^*$.

The adaptive laws of the estimated weight vectors are designed as:

$$
\dot{\hat{\boldsymbol{W}}}_4 = \Gamma_4 S_4\boldsymbol{\xi}_4 - \Gamma_4\eta_5\hat{\boldsymbol{W}}_4 \qquad (47)
$$
$$
\dot{\hat{\boldsymbol{V}}}_4 = \Gamma_{g_4} S_4\boldsymbol{\zeta}_4\dot{\gamma}_d - \Gamma_{g_4}\eta_6\hat{\boldsymbol{V}}_4 \qquad (48)
$$

Step 2. The dynamics of the pitch angle tracking error is written as:

$$
\begin{aligned}
\dot{S}_5 &= \dot{\theta} - \dot{\theta}_d \\
&= q - \dot{\theta}_d \qquad (49)
\end{aligned}
$$

A virtual control variable $\bar{q}_d$ is designed as:

$$
\bar{q}_d = -k_5 S_5 + \dot{\theta}_d \qquad (50)
$$

where $k_5 > 0$ is the gain parameter.

Introduce a new state variable q_d and let $\bar{q}_d$ pass through a first-order filter with positive time constant τ_6 to obtain q_d

$$
\tau_6\dot{q}_d + q_d = \bar{q}_d, q_d(0) = \bar{q}_d(0). \qquad (51)
$$

Define $y_6 \triangleq q_d - \bar{q}_d$, $S_6 \triangleq q - q_d$. Then, (49) is calculated as:

$$
\begin{aligned}
\dot{S}_5 &= q - \dot{\theta}_d \\
&= -k_5 S_5 + y_6 + S_6 \qquad (52)
\end{aligned}
$$

Step 3. The dynamics of the pitch angle rate tracking error is written as:

$$
\dot{S}_6 = \dot{q} - \dot{q}_d
$$

$$= f_6 + g_6\delta_e - \dot{q}_d$$
$$= g_6(g_6^{-1}f_6 + \delta_e - g_6^{-1}\dot{\gamma}_d) \quad (53)$$

Using RBF-NN to approximate the unknown function $g_6^{-1}f_6$, g_6^{-1} on the compact set Ω_{x_6}, we have

$$g_6^{-1}f_6 = \boldsymbol{W}_6^{*\mathrm{T}}\boldsymbol{\xi}_6 + \varepsilon_6^* \quad (54)$$
$$g_6^{-1} = \boldsymbol{V}_6^{*\mathrm{T}}\boldsymbol{\zeta}_6 + \delta_6^* \quad (55)$$

where $\boldsymbol{W}_6^*$, $\boldsymbol{V}_6^*$ are optimal weight vectors, $\boldsymbol{\xi}_6$, $\boldsymbol{\zeta}_6$ are the basis function vectors, ε_6^*, δ_6^* are NN approximation error, and $|\varepsilon_6^*| < \varepsilon_{6m}$, $|\delta_6^*| < \delta_{6m}$.

The control variable δ_e is designed as:

$$\delta_e = -k_6S_6 - \hat{\boldsymbol{W}}_6^{\mathrm{T}}\boldsymbol{\xi}_6 + \hat{\boldsymbol{V}}_6^{\mathrm{T}}\boldsymbol{\zeta}_6\dot{q}_d \quad (56)$$

where $k_6 > 0$ is the gain parameter, $\hat{\boldsymbol{W}}_6$ is the estimation of $\boldsymbol{W}_6^*$, and $\hat{\boldsymbol{V}}_6$ is the estimation of $\boldsymbol{V}_6^*$.

Then, (53) is calculated as:

$$\begin{aligned}\dot{S}_6 &= g_6(g_6^{-1}f_6 + \delta_e - g_6^{-1}\dot{q}_d)\\ &= g_6[\boldsymbol{W}_6^{*\mathrm{T}}\boldsymbol{\xi}_6 + \varepsilon_6^* + (-k_6S_6 - \hat{\boldsymbol{W}}_6^{\mathrm{T}}\boldsymbol{\xi}_6 + \hat{\boldsymbol{V}}_6^{\mathrm{T}}\boldsymbol{\zeta}_6\dot{q}_d)\\ &\quad - (\boldsymbol{V}_6^{*\mathrm{T}}\boldsymbol{\zeta}_6 + \delta_6^*)\dot{q}_d]\\ &= g_6[-k_6S_6 - \tilde{\boldsymbol{W}}_6^{\mathrm{T}}\boldsymbol{\xi}_6 + \tilde{\boldsymbol{V}}_6^{\mathrm{T}}\boldsymbol{\zeta}_6\dot{q}_d\\ &\quad + \varepsilon_6^* - \delta_6^*\dot{q}_d] \quad (57)\end{aligned}$$

where $\tilde{\boldsymbol{W}}_6 = \hat{\boldsymbol{W}}_6 - \boldsymbol{W}_6^*$ and $\tilde{\boldsymbol{V}}_6 = \hat{\boldsymbol{V}}_6 - \boldsymbol{V}_6^*$.

The adaptive laws of the estimated weight vectors are designed as:

$$\dot{\hat{\boldsymbol{W}}}_6 = \Gamma_6 S_6 \boldsymbol{\xi}_6 - \Gamma_6\eta_7\hat{\boldsymbol{W}}_6 \quad (58)$$
$$\dot{\hat{\boldsymbol{V}}}_6 = \Gamma_{g6}S_6\boldsymbol{\zeta}_6\dot{q}_d - \Gamma_{g6}\eta_8\hat{\boldsymbol{V}}_6 \quad (59)$$

D. STABILITY ANALYSIS

In this section, it is shown that the control scheme and adaptive laws developed in aforementioned procedures can guarantee the uniform ultimate boundedness of all signals in the close-loop system.

Theorem 1: Consider the Lyapunov function candidate

$$L \triangleq \sum_{i=1}^{6} L_i \quad (60)$$

where

$$L_1 = \frac{1}{2}(\frac{S_1^2}{g_1} + y_2^2 + \tilde{\boldsymbol{W}}_1^{\mathrm{T}}\Gamma_1^{-1}\tilde{\boldsymbol{W}}_1 + \tilde{\boldsymbol{V}}_1^{\mathrm{T}}\Gamma_{g1}^{-1}\tilde{\boldsymbol{V}}_1) \quad (61)$$

$$L_2 = \frac{1}{2}(\frac{S_2^2}{g_2} + \tilde{\boldsymbol{W}}_2^{\mathrm{T}}\Gamma_2^{-1}\tilde{\boldsymbol{W}}_2 + \tilde{\boldsymbol{V}}_2^{\mathrm{T}}\Gamma_{g2}^{-1}\tilde{\boldsymbol{V}}_2) \quad (62)$$

$$L_3 = 0 \quad (63)$$

$$L_4 = \frac{1}{2}(\frac{S_4^2}{g_4} + y_5^2 + \tilde{\boldsymbol{W}}_4^{\mathrm{T}}\Gamma_4^{-1}\tilde{\boldsymbol{W}}_4 + \tilde{\boldsymbol{V}}_4^{\mathrm{T}}\Gamma_{g4}^{-1}\tilde{\boldsymbol{V}}_4) \quad (64)$$

$$L_5 = \frac{1}{2}(S_5^2 + y_6^2) \quad (65)$$

$$L_6 = \frac{1}{2}(\frac{S_6^2}{g_6} + \tilde{\boldsymbol{W}}_6^{\mathrm{T}}\Gamma_6^{-1}\tilde{\boldsymbol{W}}_6 + \tilde{\boldsymbol{V}}_6^{\mathrm{T}}\Gamma_{g6}^{-1}\tilde{\boldsymbol{V}}_6) \quad (66)$$

where $\Gamma_{(\cdot)} = \Gamma_{(\cdot)}^{\mathrm{T}} > 0$ is given in aforementioned procedures. Given a positive number κ, for all initial conditions of (62) satisfying

$$L(0) = \sum_{i=1}^{6} L_i(0) \le \kappa \quad (67)$$

there exist $\tau_i(i = 2, 5, 6)$, $k_i(i = 1, \cdots, 6)$, $\eta_i(i = 1, \cdots, 8)$, and $\Gamma_{(\cdot)}$ such that all signals are uniformly ultimately bounded, and the tracking error converges to a residual set that can be made arbitrarily small by choosing proper design parameters.

Proof: Take derivative of L_1

$$\dot{L}_1 = \frac{S_1\dot{S}_1}{g_1} - \frac{\dot{g}_1 S_1^2}{2g_1^2} + y_2\dot{y}_2 + \tilde{\boldsymbol{W}}_1^{\mathrm{T}}\Gamma_1^{-1}\dot{\hat{\boldsymbol{W}}}_1$$
$$+ \tilde{\boldsymbol{V}}_1^{\mathrm{T}}\Gamma_{g1}^{-1}\dot{\hat{\boldsymbol{V}}}_1 \quad (68)$$

From (28), we have

$$\dot{y}_2 = \dot{V}_d - \dot{\bar{V}}_d = -\frac{y_2}{\tau_2} + B_2 \quad (69)$$

where $B_2 = \dot{\bar{V}}_d$ and the upper bound of $|B_2|$ is M_2. Hence,

$$\dot{y}_2 y_2 \le -\frac{y_2^2}{\tau_2} + B_2|y_2| \quad (70)$$

Using (70), and substituting (29) and adaptive laws (30), (31) in (68), we have

$$\dot{L}_1 \le -k_1S_1^2 - \frac{\dot{g}_1}{2g_1^2}S_1^2 + S_1S_2 + S_1y_2 - \frac{y_2^2}{\tau_2} + B_2|y_2|$$
$$+ S_1(\varepsilon_1^* - \delta_1^*\dot{x}_d) - \eta_1\tilde{\boldsymbol{W}}_1^{\mathrm{T}}\hat{\boldsymbol{W}}_1 - \eta_2\tilde{\boldsymbol{V}}_1^{\mathrm{T}}\hat{\boldsymbol{V}}_1 \quad (71)$$

Define $e_1^* \triangleq \varepsilon_1^* - \delta_1^*\dot{x}_d$ and let $e_{1M} > 0$ such that $|e_1^*| < e_{1M}$. Therefore,

$$\dot{L}_1 \le -k_1S_1^2 - \frac{\dot{g}_1}{2g_1^2}S_1^2 + S_1S_2 + S_1y_2 - \frac{y_2^2}{\tau_2} + B_2|y_2|$$
$$+ S_1e_{1M} - \eta_1\tilde{\boldsymbol{W}}_1^{\mathrm{T}}\hat{\boldsymbol{W}}_1 - \eta_2\tilde{\boldsymbol{V}}_1^{\mathrm{T}}\hat{\boldsymbol{V}}_1 \quad (72)$$

Note that $ab \le \frac{1}{2}a^2 + \frac{1}{2}b^2$ and $-\eta\tilde{\boldsymbol{W}}^{\mathrm{T}}\hat{\boldsymbol{W}} \le -\frac{\eta}{2}(\|\tilde{\boldsymbol{W}}\|^2 - \|\boldsymbol{W}^*\|^2)$, (72) satisfies

$$\begin{aligned}\dot{L}_1 \le &-(k_1 + \frac{g_{1c}}{2g_1^2} - \frac{3}{2})S_1^2 + \frac{S_2^2}{2} - (\frac{1}{\tau_2} - 1)y_2^2 + \frac{M_2^2}{2}\\ &+ \frac{e_{1M}^2}{2} - \frac{\eta_1}{2}\|\tilde{\boldsymbol{W}}_1\|^2 + \frac{\eta_1}{2}\|\boldsymbol{W}_1^*\|^2 - \frac{\eta_2}{2}\|\tilde{\boldsymbol{V}}_1\|^2\\ &+ \frac{\eta_2}{2}\|\boldsymbol{V}_1^*\|^2\end{aligned}$$

$$\begin{aligned}\le &-(k_1 + \frac{g_{1c}}{2g_1^2} - \frac{3}{2})S_1^2 + \frac{S_2^2}{2} - (\frac{1}{\tau_2} - 1)y_2^2 + \frac{M_2^2}{2}\\ &+ \frac{e_{1M}^2}{2} - \frac{\eta_1}{2\lambda_{max}(\Gamma_1^{-1})}\tilde{\boldsymbol{W}}_1^{\mathrm{T}}\Gamma_1^{-1}\tilde{\boldsymbol{W}}_1 + \frac{\eta_1}{2}\|\boldsymbol{W}_1^*\|^2\\ &- \frac{\eta_2}{2\lambda_{max}(\Gamma_{g1}^{-1})}\tilde{\boldsymbol{V}}_1^{\mathrm{T}}\Gamma_{g1}^{-1}\tilde{\boldsymbol{V}}_1 + \frac{\eta_2}{2}\|\boldsymbol{V}_1^*\|^2\end{aligned}$$

$$\le -\gamma_1[\frac{1}{g_1}S_1^2 + \tilde{\boldsymbol{W}}_1^{\mathrm{T}}\Gamma_1^{-1}\tilde{\boldsymbol{W}}_1 + \tilde{\boldsymbol{V}}_1^{\mathrm{T}}\Gamma_{g1}^{-1}\tilde{\boldsymbol{V}}_1 + y_2^2]$$

$$+ C_1 + \frac{S_2^2}{2}$$

$$= -2\gamma_1 L_1 + C_1 + \frac{S_2^2}{2} \tag{73}$$

where $\lambda_{max}(\cdot)$ is the maximum eigenvalue of $(\cdot)$ and

$$0 < \gamma_1 < \min[K_1, \frac{\eta_1}{2\lambda_{max}(\Gamma_1^{-1})}, \frac{\eta_2}{2\lambda_{max}(\Gamma_{g1}^{-1})}, \frac{1}{\tau_2} - 1]$$

$$K_1 = (k_1 + \frac{g_{1c}}{2g_1^2} - \frac{3}{2})g_{1m} > 0$$

$$C_1 = \frac{M_2^2}{2} + \frac{e_{1M}^2}{2} + \frac{\eta_1}{2}\|W_1^*\|^2 + \frac{\eta_2}{2}\|V_1^*\|^2$$

Similarly, define $e_2^* \triangleq \varepsilon_2^* - \delta_2^* \dot{V}_d$ and let $e_{2M} > 0$ such that $|e_2^*| < e_{2M}$. Therefore,

$$\dot{L}_2 \leq -(k_2 + \frac{g_{2c}}{2g_2^2} - 1)S_2^2 - \frac{S_2^2}{2} + \frac{e_{2M}^2}{2}$$

$$- \frac{\eta_3}{2\lambda_{max}(\Gamma_2^{-1})}\tilde{W}_2^\mathrm{T}\Gamma_2^{-1}\tilde{W}_2 + \frac{\eta_3}{2}\|W_2^*\|^2$$

$$- \frac{\eta_4}{2\lambda_{max}(\Gamma_{g2}^{-1})}\tilde{V}_2^\mathrm{T}\Gamma_{g2}^{-1}\tilde{V}_2 + \frac{\eta_4}{2}\|V_2^*\|^2$$

$$\leq -\gamma_2[\frac{1}{g_2}S_2^2 + \tilde{W}_2^\mathrm{T}\Gamma_2^{-1}\tilde{W}_2 + \tilde{V}_2^\mathrm{T}\Gamma_{g2}^{-1}\tilde{V}_2]$$

$$+ C_2 - \frac{S_2^2}{2}$$

$$= -2\gamma_2 L_2 + C_2 - \frac{S_2^2}{2} \tag{74}$$

where

$$0 < \gamma_2 < \min[K_2, \frac{\eta_3}{2\lambda_{max}(\Gamma_2^{-1})}, \frac{\eta_4}{2\lambda_{max}(\Gamma_{g2}^{-1})}]$$

$$K_2 = (k_2 + \frac{g_{2c}}{2g_2^2} - 1)g_{2m} > 0$$

$$C_2 = \frac{e_{2M}^2}{2} + \frac{\eta_3}{2}\|W_2^*\|^2 + \frac{\eta_4}{2}\|V_2^*\|^2$$

Also define $e_4^* \triangleq \varepsilon_4^* - \delta_4^* \dot{\gamma}_d$ and let $e_{4M} > 0$ such that $|e_4^*| < e_{4M}$. Therefore,

$$\dot{L}_4 \leq -(k_4 + \frac{g_{4c}}{2g_4^2} - \frac{3}{2})S_4^2 + \frac{S_5^2}{2} - (\frac{1}{\tau_5} - 1)y_5^2 + \frac{M_5^2}{2}$$

$$+ \frac{e_{4M}^2}{2} - \frac{\eta_5}{2\lambda_{max}(\Gamma_4^{-1})}\tilde{W}_4^\mathrm{T}\Gamma_4^{-1}\tilde{W}_4 + \frac{\eta_5}{2}\|W_4^*\|^2$$

$$- \frac{\eta_6}{2\lambda_{max}(\Gamma_{g4}^{-1})}\tilde{V}_4^\mathrm{T}\Gamma_{g4}^{-1}\tilde{V}_4 + \frac{\eta_6}{2}\|V_4^*\|^2$$

$$\leq -\gamma_4[\frac{1}{g_4}S_4^2 + \tilde{W}_4^\mathrm{T}\Gamma_4^{-1}\tilde{W}_4 + \tilde{V}_4^\mathrm{T}\Gamma_{g4}^{-1}\tilde{V}_4 + y_5^2]$$

$$+ C_4 + \frac{S_5^2}{2}$$

$$= -2\gamma_4 L_4 + C_4 + \frac{S_5^2}{2} \tag{75}$$

where

$$0 < \gamma_4 < \min[K_4, \frac{\eta_5}{2\lambda_{max}(\Gamma_4^{-1})}, \frac{\eta_6}{2\lambda_{max}(\Gamma_{g4}^{-1})}, \frac{1}{\tau_5} - 1]$$

$$K_4 = (k_4 + \frac{g_{4c}}{2g_4^2} - \frac{3}{2})g_{4m} > 0$$

$$C_4 = \frac{M_5^2}{2} + \frac{e_{4M}^2}{2} + \frac{\eta_5}{2}\|W_4^*\|^2 + \frac{\eta_6}{2}\|V_4^*\|^2$$

And,

$$\dot{L}_5 \leq -(k_5 - \frac{3}{2})S_5^2 - \frac{S_5^2}{2} + \frac{S_6^2}{2} - (\frac{1}{\tau_6} - 1)y_6^2 + \frac{M_6^2}{2}$$

$$\leq -\gamma_5(S_5^2 + y_6^2) + C_5 - \frac{S_5^2}{2} + \frac{S_6^2}{2}$$

$$= -2\gamma_5 L_5 + C_5 - \frac{S_5^2}{2} + \frac{S_6^2}{2} \tag{76}$$

where

$$0 < \gamma_5 < \min[K_5 \frac{1}{\tau_6} - 1]$$

$$K_5 = k_5 - \frac{3}{2} > 0, \quad C_5 = \frac{M_6^2}{2}$$

Also define $e_6^* \triangle \varepsilon_6^* - \delta_6^* \dot{q}_d$ and let $e_{6M} > 0$ such that $|e_6^*| < e_{6M}$. Therefore,

$$\dot{L}_6 \leq -(k_6 + \frac{g_{6c}}{2g_6^2} - 1)S_6^2 - \frac{S_6^2}{2} + \frac{e_{6M}^2}{2}$$

$$- \frac{\eta_7}{2\lambda_{max}(\Gamma_6^{-1})}\tilde{W}_6^\mathrm{T}\Gamma_6^{-1}\tilde{W}_6 + \frac{\eta_7}{2}\|W_6^*\|^2$$

$$- \frac{\eta_8}{2\lambda_{max}(\Gamma_{g6}^{-1})}\tilde{V}_6^\mathrm{T}\Gamma_{g6}^{-1}\tilde{V}_6 + \frac{\eta_8}{2}\|V_6^*\|^2$$

$$\leq -\gamma_6[\frac{1}{g_6}S_6^2 + \tilde{W}_6^\mathrm{T}\Gamma_6^{-1}\tilde{W}_6 + \tilde{V}_6^\mathrm{T}\Gamma_{g6}^{-1}\tilde{V}_6]$$

$$+ C_6 - \frac{S_6^2}{2}$$

$$= -2\gamma_6 L_6 + C_6 - \frac{S_6^2}{2} \tag{77}$$

where

$$0 < \gamma_6 < \min[K_6, \frac{\eta_7}{2\lambda_{max}(\Gamma_6^{-1})}, \frac{\eta_8}{2\lambda_{max}(\Gamma_{g6}^{-1})}]$$

$$K_6 = (k_6 + \frac{g_{6c}}{2g_6^2} - 1)g_{6m} > 0$$

$$C_6 = \frac{e_{6M}^2}{2} + \frac{\eta_7}{2}\|W_6^*\|^2 + \frac{\eta_8}{2}\|V_6^*\|^2$$

From (73)–(77), we have

$$\dot{L} \leq \sum_{i \neq 3}(-2\gamma_i L_i + C_i) \leq -2\varpi L + C, \tag{78}$$

where $\varpi = \min[\gamma_1, \gamma_2, \gamma_4, \gamma_5, \gamma_6]$ and $C = \sum_{i \neq 3} C_i$. If $L = \kappa$, then $\dot{L} < 0$ when $\varpi > \frac{C}{2\kappa}$. Thus, given $L(0) < \kappa$, we have $L(t) \leq \kappa, \forall t \geq 0$. Moreover, by solving (78), we can obtain

$$0 \leq L \leq \frac{C}{2\varpi} + (L(0) - \frac{C}{2\varpi})e^{-2\varpi t} \tag{79}$$

Furthermore,

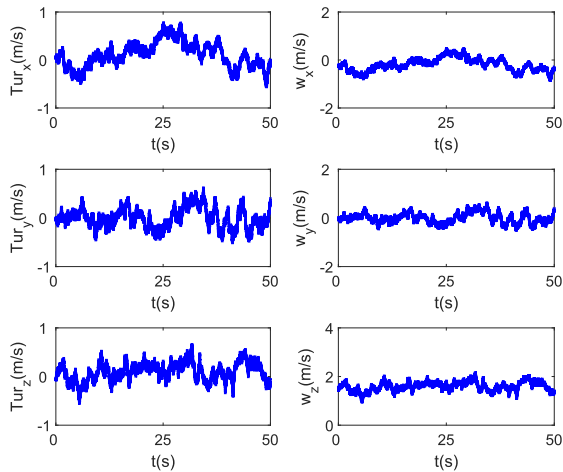$$\lim_{t \to \infty} L(t) \leq \frac{C}{2\varpi} \tag{80}$$

FIGURE 6. External disturbances.

By properly choosing control parameters $\tau_i(i = 2, 5, 6)$, $k_i(i = 1, 2, 4, 5, 6)$, $\eta_i(i = 1, \cdots, 8)$ and $\Gamma_{(.)}$, we can make ϖ sufficiently large, which ensures that the close-loop system stability is uniformly ultimately bounded and the tracking error S_1 and S_4 can converge to an arbitrarily small residual set. This completes the proof.

IV. SIMULATION RESULTS AND ANALYSES

In this section, the simulation results of the receiver longitudinal docking control are analysed to demonstrate the validity of the proposed NN-ADSC controller. The tanker aircraft is assumed to fly in level flight with $V_T = 180$ m/s, $H_T = 7010$ m, and the receiver aircraft adopted in the simulation is an equivalent model for innovative control effectors (ICE) in [38]. The parameters of the ICE are listed in Appendix A and the model uncertainties are considered as the random numbers. In addition, the conventional DSC control scheme are chosen to make comparisons.

For all numerical simulations presented below, the initial flight conditions of the receiver are $x(0) = $ -66 m, $y(0) = 0$ m, $z(0) = 15$ m, $V(0) = 180$ m/s, $\alpha(0) = 0.03$ rad, $\theta(0) = 0.03$ rad, $\gamma(0) = 0$ rad, $q(0) = 0$ rad/s. The initial values of the vortex model are selected as $w_x = $ -0.22 m/s, $w_z = 1.5$ m/s, $q_d = $ -0.2 rad/s. The controller parameters are chosen as $k_1 = 2$, $k_2 = 2.5$, $k_{31} = 3.2$, $k_{32} = 0.2$, $k_4 = 10$, $k_5 = 3$, $k_6 = 2$, $\tau_2 = \tau_5 = \tau_6 = 0.05$, $\eta_i = 0.01$ ($i = 1, \cdots, 8$), $\Gamma_i = \Gamma_{g_i} = diag\{50\}$ ($i = 1, 2, 4, 6$). The number of NN nodes is set as $N_1 = 3 \times 7$, $N_i = 7$ ($i = 2, 4, 6, 8$), and $N_j = 3 \times 7 \times 7 \times 3$ ($j = 3, 5, 7$).

In the simulation, the receiver approaches the tanker from pre-contact position ($x_r = $ -66 m, $y_r = 0$ m, $z_r = 15$ m) to contact position ($x_r = $ -21 m, $y_r = 0$ m, $z_r = 7$ m) in 50 s, where (x_r, y_r, z_r) are the reference signals of the receiver position with respect to the tanker and the reference signals end at the equilibrium point of the moving drogue. To verify the external disturbances attenuation ability of the proposed NN-ADSC scheme, the receiver is assumed to encounter the light turbulence and vortex in the simulation study. The
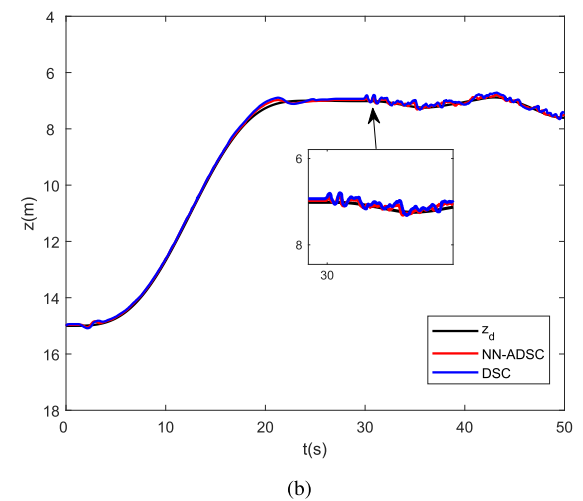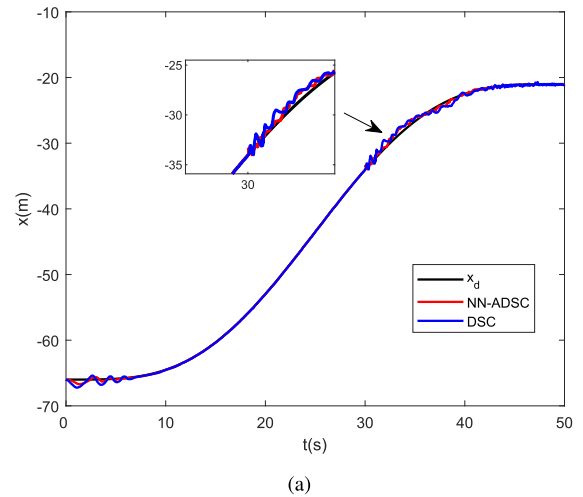

(a)

(b)

FIGURE 7. Position tracking results of the receiver with respect to the tanker.

turbulence and the total effect of the turbulence and vortex wind are shown in Fig. 6.

The nonlinear close-loop simulation results for the receiver longitudinal tracking are shown in Fig. 7 to Fig. 10. To show explicitly the advantages of the proposed controller, the position tracking together with tracking errors in each axis of proposed controller and conventional DSC controller are contrastively presented in Fig. 7 (a), Fig. 7 (b), and Fig. 8. We notice that both the proposed NN-ADSC and DSC can guarantee the relative forward distance and altitude to follow the designed smooth reference docking trajectory. But there are still some differences between two controllers, NN-ADSC has obviously better tracking performance especially when the random uncertainties of dynamics are incorporated into the simulation from $t = 30$ s, which can be easily seen in Fig. 7 and Fig. 8. From $t = 30$ s, the receiver is particularly close to the tanker and its dynamic parameters are rapidly changed because of the aerodynamic coupling effect between two aircrafts. Thus, the tracking errors increase significantly, and the
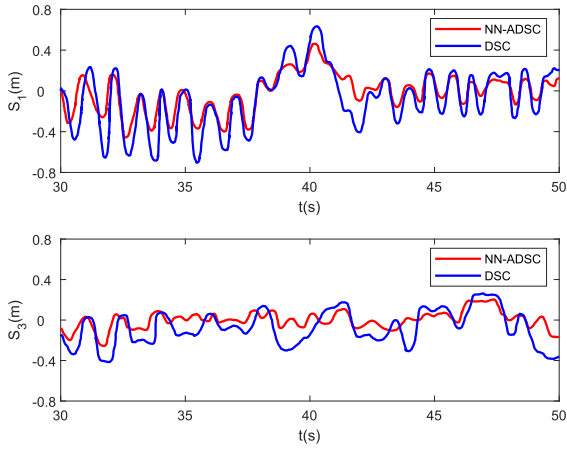
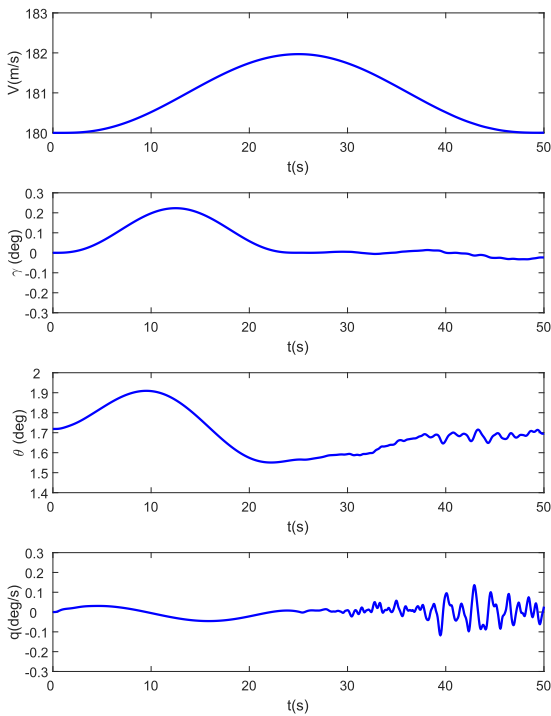**FIGURE 8.** Position tracking errors of the receiver.

FIGURE 9. Simulation results for states of the receiver.

simulation results in Fig. 8 shows that the receiver's position fluctuates around the reference trajectory, but the errors S_1, S_3 are bounded during the entire approaching process. The NN-ADSC controller can ensure the tracking error within the desired error threshold $R_c = 0.2$ m, while the DSC's threshold is larger as $R_c = 0.4$ m.

Fig. 9 shows the time responses of the system states, including velocity, path angle, pitch angle, and pitch angle rate. It can be observed that all system states are uniformly ultimately bounded with NN-ADSC, and converge to a new steady flight condition where the velocity and path angle are identical to the nominal condition, but the pitch angle and its rate change rapidly to compensate the effects of external disturbances.
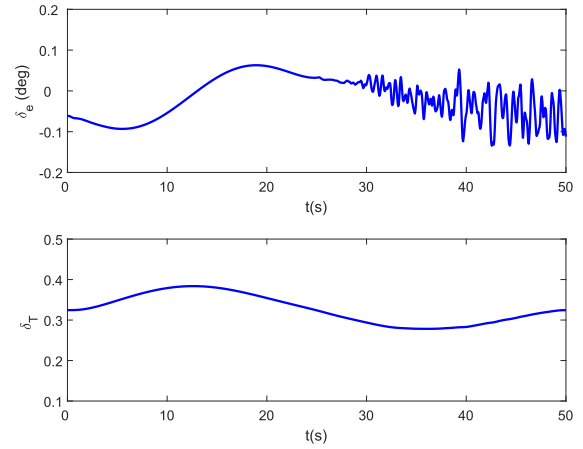

FIGURE 10. Simulation results for control inputs of the receiver.

Fig. 10 illustrates the time responses of thrust throttle setting and elevator input signals. It can be found that the receiver pulls up and accelerates to follow the reference trajectory in the first stage (0 s − 30 s), and in the second stage (30 s − 50 s) the elevator control input changes to ensure the receiver can capture the moving drogue in z direction with the presence of the disturbances. Besides, all control input signals are uniformly ultimately bounded and within the aircraft capability limitations as well.

V. CONCLUSION

In this paper, a new NN-ADSC scheme is presented for AAR docking controller design. The scheme has a systematic design theory to achieve uniformly ultimately bounded performance for all system signals. Based on a longitudinal dynamic model of ICE, the NN-ADSC control scheme is designed to realize the PDR docking under external disturbances and model uncertainties. The main feature of the scheme is the use of RBF neural networks to adaptively approximate the time-varying system parameters. A smooth reference trajectory is also designed to get satisfactory transient process. The comparatively simulations between the proposed scheme and conventional DSC have revealed that the NN-ADSC can not only effectively reduce relative position errors between the receiver and the drogue, but also ensure all signals uniformly ultimately bounded. In a word, the proposed NN-ADSC improves the docking ability under disturbances and uncertainties. Nevertheless, the lateral dynamics of the receiver has not been considered in the controller design because it is assumed in current application experience that the receiver only needs to make longitudinal maneuvers. However, to make the research more practical, the lateral stabilization system will be considered in the future work.

APPENDIX A

Expressions of force and moment in the receiver model:

$$\bar{q} = \frac{1}{2}\rho V^2, \quad q_{rel} = q - q_d, \quad \mathcal{D} = \bar{q}S_r C_{\mathcal{D}}, \quad \mathcal{L} = \bar{q}S_r C_{\mathcal{L}},$$

$$\mathcal{M} = \bar{q} S_r \bar{c} C_\mathcal{M}, \quad \mathcal{T} = \mathcal{T}_{max} \delta_T,$$
$$C_\mathcal{D} = C_{\mathcal{D}_0} + C_{\mathcal{D}_{\alpha 2}} \alpha^2, \quad C_\mathcal{L} = C_{\mathcal{L}_0} + C_{\mathcal{L}_\alpha} \alpha,$$
$$C_\mathcal{M} = C_{\mathcal{M}_0} + C_{\mathcal{M}_\alpha} \alpha + C_{\mathcal{M}_{\delta_e}} \delta_e + C_{\mathcal{M}_q} \frac{\bar{c} q_{rel}}{2V},$$
$$C_{\mathcal{M}_q} = C_{\mathcal{M}_q}^0 + C_{\mathcal{M}_q}^\alpha \alpha + C_{\mathcal{M}_q}^{\alpha 2} \alpha^2 + C_{\mathcal{M}_q}^{\alpha 3} \alpha^3.$$

Receiver aircraft (ICE) parameters used in the simulations:

$m = 1.4842 \times 10^4$ kg, $S_r = 72.7722$ m^2, $\bar{c} = 5.6789$ m, $\rho = 0.5903$ kg $\cdot$ m^{-3}, $g = 9.8$ m $\cdot$ s^{-2}, $I_y = 1.0308 \times 10^5$ kg $\cdot$ m^2, $\mathcal{T}_{max} = 24916$ N,

$C_{\mathcal{D}_0} = 0.0102$, $C_{\mathcal{D}_{\alpha 2}} = 1.5684$, $C_{\mathcal{L}_0} = -0.0008$, $C_{\mathcal{L}_\alpha} = 4.4955$, $C_{\mathcal{M}_0} = 0$, $C_{\mathcal{M}_\alpha} = -0.0969$, $C_{\mathcal{M}_{\delta_e}} = -0.0436$, $C_{\mathcal{M}_q}^0 = -1.2094$, $C_{\mathcal{M}_q}^\alpha = -0.0266$, $C_{\mathcal{M}_q}^{\alpha 2} = 0.6001$, $C_{\mathcal{M}_q}^{\alpha 3} = 1.6224$.

APPENDIX B

Variables in (7) – (12):

$$g_1 = \cos\gamma, \quad f_1 = -V_T + w_x \cos\theta + w_z \sin\theta,$$
$$g_2 = \frac{\mathcal{T}_{max} \cos\alpha}{m},$$
$$f_2 = -\frac{\bar{q} S_r}{m}(C_{\mathcal{D}_0} + C_{\mathcal{D}_{\alpha 2}} \alpha^2) - g\sin\gamma$$
$$- (\dot{w}_x + q w_z)\cos\alpha + (q w_x - \dot{w}_z)\sin\alpha,$$
$$g_3 = -V, \quad f_3 = w_z \cos\theta - w_x \sin\theta,$$
$$g_4 = \frac{\bar{q} S_r C_{\mathcal{L}_\alpha}}{mV},$$
$$f_4 = \frac{-mg\cos\gamma + \bar{q} S_r C_{\mathcal{L}_0} - \bar{q} S_r C_{\mathcal{L}_\alpha} \gamma}{mV}$$
$$- \frac{w_x q \cos(\theta - \gamma) + w_z g \sin(\theta - \gamma)}{V}$$
$$+ \frac{\dot{w}_x \sin(\theta - \gamma) - \dot{w}_z \cos(\theta - \gamma)}{V},$$
$$g_6 = \frac{\bar{q} S_r \bar{c} C_{\mathcal{M}_{\delta_e}}}{I_y}, f_6 = \frac{\bar{q} S_r \bar{c}(C_{\mathcal{M}_0} + C_{\mathcal{M}_\alpha} \alpha + C_{\mathcal{M}_q} \frac{\bar{c} q_{rel}}{2V})}{I_y}.$$

REFERENCES

[1] P. R. Thomas, U. Bhandari, S. Bullock, T. S. Richardson, and J. L. du Bois, "Advances in air to air refuelling," *Prog. Aerosp. Sci.*, vol. 71, pp. 14–35, Nov. 2014.

[2] R. Dibley, M. Allen, and N. Nabaa, "Autonomous airborne refueling demonstration phase I flight-test results," in *Proc. AIAA Atmos. Flight Mech. Conf. Exhib.*, Hilton Head, SC, USA, Aug. 2007, p. 6639.

[3] J. P. Nalepka and J. L. Hinchman, "Automated aerial refueling: Extending the effectiveness of unmanned air vehicles," in *Proc. AIAA Modeling Simulation Technol. Conf. Exhib.*, San Francisco, CA, USA, Aug. 2005, pp. 240–247.

[4] Y. Yin, X. Wang, D. Xu, F. Liu, Y. Wang, and W. Wu, "Robust visual detection–learning–tracking framework for autonomous aerial refueling of UAVs," *IEEE Trans. Instrum. Meas.*, vol. 65, no. 3, pp. 510–521, Mar. 2016.

[5] Y. Ma, R. Zhao, E. Liu, Z. Zhang, and K. Yan, "A novel method for measuring drogue-UAV relative pose in autonomous aerial refueling based on monocular vision," *IEEE Access*, vol. 7, pp. 139653–139667, Sep. 2019.

[6] J. Ren, X. Dai, Q. Quan, Z.-B. Wei, and K.-Y. Cai, "Reliable docking control scheme for probe–drogue refueling," *J. Guid., Control, Dyn.*, vol. 42, no. 11, pp. 2511–2520, Nov. 2019.

[7] Z.-B. Wei, X. Dai, Q. Quan, and K.-Y. Cai, "Drogue dynamic model under bow wave in probe-and-drogue refueling," *IEEE Trans. Aerosp. Electron. Syst.*, vol. 52, no. 4, pp. 1728–1742, Aug. 2016.

[8] M. Bolien, P. Iravani, and J. L. D. Bois, "Toward robotic pseudodynamic testing for hybrid simulations of air-to-air refueling," *IEEE/ASME Trans. Mechatronics*, vol. 22, no. 2, pp. 1004–1013, Apr. 2017.

[9] *ATP-56 (B) Air-to-Air Refuelling*, NATO TR ATP 3.3.4.2, Brussels, Belgium, 2010.

[10] M. L. Fravolini, A. Ficola, G. Campa, M. R. Napolitano, and B. Seanor, "Modeling and control issues for autonomous aerial refueling for UAVs using a probe–drogue refueling system," *Aerosp. Sci. Technol.*, vol. 8, pp. 611–618, Oct. 2004.

[11] E. Kim, A. Dogan, and W. Blake, "Control of a receiver aircraft relative to the tanker in racetrack maneuver," in *Proc. AIAA Guid., Navigat., Control Conf. Exhib.*, Keystone, CO, USA, Aug. 2006, p. 6710.

[12] G. Campa, M. R. Napolitano, and M. L. Fravolini, "Simulation environment for machine vision based aerial refueling for UAVs," *IEEE Trans. Aerosp. Electron. Syst.*, vol. 45, no. 1, pp. 138–151, Jan. 2009.

[13] S. Wu, L. Zhang, W. Xu, T. Zhou, and D. Luo, "Docking control of autonomous aerial refueling for UAV based on LQR," in *Proc. 10th IEEE Int. Conf. Control Autom. (ICCA)*, Hangzhou, China, Jun. 2013, pp. 1819–1823.

[14] J. Wang, V. Patel, C. Cao, N. Hovakimyan, and E. Lavretsky, "L1 adaptive neural network controller for autonomous aerial refueling with guaranteed transient performance," in *Proc. AIAA Guid., Navigat., Control Conf. Exhib.*, Keystone, CO, USA, Aug. 2006, p. 6206.

[15] J. Wang, V. V. Patel, C. Cao, N. Hovakimyan, and E. Lavretsky, "Novel L1 adaptive control methodology for aerial refueling with guaranteed transient performance," *J. Guid., Control, Dyn.*, vol. 31, no. 1, pp. 182–193, Jan. 2008.

[16] M. Herrnberger, G. Sachs, F. Holzapfel, W. Tostmann, and E. Weixler, "Simulation analysis of autonomous aerial refueling procedures," in *Proc. AIAA Guid., Navigat., Control Conf. Exhib.*, San Francisco, CA, USA, Aug. 2005, p. 5866.

[17] J. O. Pedro, A. Panday, and L. Dala, "A nonlinear dynamic inversion-based neurocontroller for unmanned combat aerial vehicles during aerial refuelling," *Int. J. Appl. Math. Comput. Sci.*, vol. 23, no. 1, pp. 75–90, Mar. 2013.

[18] Z. Su, H. Wang, P. Yao, Y. Huang, and Y. Qin, "Back-stepping based anti-disturbance flight controller with preview methodology for autonomous aerial refueling," *Aerosp. Sci. Technol.*, vol. 61, pp. 95–108, Feb. 2017.

[19] Z. Su, H. Wang, X. Shao, and P. Yao, "Autonomous aerial refueling precise docking based on active disturbance rejection control," in *Proc. IECON-41st Annu. Conf. IEEE Ind. Electron. Soc.*, Yokohama, Japan, Nov. 2015, pp. 004574–004578.

[20] J.-M. Lou and K. Zhang, "Design of active disturbance rejection controller for autonomous aerial refueling UAV," in *Proc. IEEE Int. Conf. IEEE Region 10 (TENCON)*, Xi'an, China, Oct. 2013, pp. 1–4.

[21] Z. Su, H. Wang, N. Li, Y. Yu, and J. Wu, "Exact docking flight controller for autonomous aerial refueling with back-stepping based high order sliding mode," *Mech. Syst. Signal Process.*, vol. 101, pp. 338–360, Feb. 2018.

[22] J. Valasek, D. Famularo, and M. Marwaha, "Fault-tolerant adaptive model inversion control for vision-based autonomous air refueling," *J. Guid., Control, Dyn.*, vol. 40, no. 6, pp. 1336–1347, Jun. 2017.

[23] Z. Yu, Y. Qu, and Y. Zhang, "Safe control of trailing UAV in close formation flight against actuator fault and wake vortex effect," *Aerosp. Sci. Technol.*, vol. 77, pp. 189–205, Jun. 2018.

[24] X. Dai, Q. Quan, J. Ren, Z. Xi, and K. Y. Cai, "Terminal iterative learning control for autonomous aerial refueling under aerodynamic disturbances," *J. Guid., Control, Dyn.*, vol. 41, no. 7, pp. 1576–1584, Jul. 2018.

[25] D. Swaroop, J. K. Hedrick, P. P. Yip, and J. C. Gerdes, "Dynamic surface control for a class of nonlinear systems," *IEEE Trans. Autom. Control*, vol. 45, no. 10, pp. 1893–1899, Oct. 2000.

[26] D. Wang and J. Huang, "Neural network-based adaptive dynamic surface control for a class of uncertain nonlinear systems in strict-feedback form," *IEEE Trans. Neural Netw.*, vol. 16, no. 1, pp. 195–202, Jan. 2005.

[27] W. A. Butt, L. Yan, and S. K. Amezquita, "Robust adaptive dynamic surface control of a hypersonic flight vehicle," in *Proc. 49th IEEE Conf. Decis. Control (CDC)*, Atlanta, GA, USA, Dec. 2010, pp. 3632–3637.

[28] B. Xu, C. Yang, and Y. Pan, "Global neural dynamic surface tracking control of strict-feedback systems with application to hypersonic flight vehicle," *IEEE Trans. Neural Netw. Learn. Syst.*, vol. 26, no. 10, pp. 2563–2575, Oct. 2015.

[29] B. Xu, L. Yu, S. Wang, and X. Feng, "Neural dynamic surface hypersonic flight control using minimal-learning-parameter technique," in *Proc. Int. Conf. Unmanned Aircr. Syst. (ICUAS)*, Orlando, FL, USA, May 2014, pp. 960–966.

[30] Z. Peng, D. Wang, Z. Chen, X. Hu, and W. Lan, "Adaptive dynamic surface control for formations of autonomous surface vehicles with uncertain dynamics," *IEEE Trans. Control Syst. Technol.*, vol. 21, no. 2, pp. 513–520, Mar. 2013.

[31] G. Zhang and X. Zhang, "Concise robust adaptive path-following control of underactuated ships using DSC and MLP," *IEEE J. Ocean. Eng.*, vol. 39, no. 4, pp. 685–694, Oct. 2014.

[32] J. Huang, S. Ri, L. Liu, Y. Wang, J. Kim, and G. Pak, "Nonlinear disturbance observer-based dynamic surface control of mobile wheeled inverted pendulum," *IEEE Trans. Control Syst. Technol.*, vol. 23, no. 6, pp. 2400–2407, Nov. 2015.

[33] D.-H. T. Kim, T.-N. Manh, N.-P. Van Bach, and T.-P. Duc, "Trajectory tracking control for omnidirectional mobile robots using direct adaptive neural network dynamic surface controller," in *Proc. 1st Int. Symp. Instrum., Control, Artif. Intell., Robot. (ICA-SYMP)*, Bangkok, Thailand, Jan. 2019, pp. 127–130.

[34] A. Dogan, S. Venkataramanan, and W. Blake, "Modeling of aerodynamic coupling between aircraft in close proximity," *J. Aircr.*, vol. 42, no. 4, pp. 941–955, Jul. 2005.

[35] K. Ro and J. W. Kamman, "Modeling and simulation of hose-paradrogue aerial refueling systems," *J. Guid., Control, Dyn.*, vol. 33, no. 1, pp. 53–63, Jan. 2010.

[36] J. Park and I. W. Sandberg, "Universal approximation using radial-basis-function networks," *Neural Comput.*, vol. 3, no. 2, pp. 246–257, Jun. 1991.

[37] R. M. Sanner and J.-J.-E. Slotine, "Gaussian networks for direct adaptive control," *IEEE Trans. Neural Netw.*, vol. 3, no. 6, pp. 837–863, Nov. 1992.

[38] A. Barfield and J. Hinchman, "An equivalent model for UAV automated aerial refueling research," in *Proc. AIAA Modeling Simulation Technol. Conf. Exhib.*, San Francisco, CA, USA, Aug. 2005, p. 6006.

HUANGDI LUO received the bachelor's degree in aircraft design and engineering from Beihang University, Beijing, China, in 2012. He is currently pursuing the Ph.D. degree in flight dynamics and flight control with Fudan University. He worked for Comac as an Engineer, from 2012 to 2015. His research interests include aircraft icing modeling and nonlinear control theory.

JIAZHENG WU received the B.Eng. degree in flight system design and engineering from Fudan University, Shanghai, China, in 2014, where he is currently pursuing the Ph.D. degree in flight dynamics and flight control. He visited the Institute of Flight System and Dynamics (FSD), Technical University of Munich (TUM), Munich, Germany, as a Ph.D. candidate, from 2017 to 2019. His research interests include aerial refueling modeling and adaptive control theory.

JIANLIANG AI received the bachelor's, master's, and the Ph.D. degrees in aircraft design from Northwestern Polytechnical University, Xi'an, China, in 1986, 1989, and 1997, respectively. He visited the Moscow State Aviation Institute as a Visiting Scholar, from 1996 to 1997. He is currently a Professor with the Department of Aeronautics and Astronautics, Fudan University. His current research interests include aircraft design and nonlinear control and intelligent control with application on flight dynamics.

• • •